Journal of Nuclear Materials 392 (2009) 78–84

Contents lists available at ScienceDirect

Journal of Nuclear Materials

journal homepage: www.elsevier.com/locate/jnucmat

An advanced model for grain face diffusion transport in irradiated UO_2 fuel. Part 1: Model formulation

M.S. Veshchunov *, V.I. Tarasov

Nuclear Safety Institute (IBRAE), Russian Academy of Sciences, 52, B. Tulskaya, Moscow 115191, Russian Federation

A B S T R A C T

An advanced model for the grain face transport of gas atoms, self-consistently taking into consideration the effects of atom diffusion over the grain surface, their trapping by and irradiation induced resolution from intergranular bubbles is presented. The model allows prediction of a noticeable gas release from UO_2 fuel without visible interlinkage of grain face bubbles, i.e. at very low grain face coverage, below the critical value manifested by formation of bubble channels on grain faces interconnected with open porosity, in accordance with experimental observations of UO_2 and MOX fuel behaviour under various irradiation conditions.

1. Introduction

In the majority of the currently existing models for fission product (FP) release from UO_2 fuel, it is assumed that the gas arriving at grain boundaries eventually saturates the grain boundaries through a network of interconnected bubbles [1–5]. The onset of gas saturation on the grain boundary is explained by a percolation mechanism, where a network of interconnected bubbles sets in at a certain concentration of gas particles on the grain faces [6]. After attainment of the saturation coverage manifested by formation of channels (or bubble chains) on the grain faces interconnected with the open porosity (escape tunnels at the grain edges), gas release (venting) from face bubbles through the channels commences.

The saturation coverage in different models is usually a fixed value corresponding to some experimental observations; however, this value is different in various models. For instance, in some models (e.g. [1,2]) this value corresponds to the face coverage of ≈0.25, whereas in other models this value is often chosen corresponding to the geometrical interlinkage condition for the regularly arranged bubbles, $\pi/4 \approx 0.79$ (e.g. [3–5]). In the VICTORIA code [7] the saturation coverage is fixed at 0.5, this value is in a good correspondence with the 2-d percolation threshold for an infinite assembly of equisized bubbles randomly distributed over the plane surface.

However, in analytical tests [8,9] where gas release from the irradiated fuel was measured simultaneously with analysis of fuel microstructure and grain face porosity, the conclusion concerning formation of percolation channels at grain faces providing commencement of gas release, was not confirmed. It was observed that a noticeable gas release from fuel took place at a rather low coverage and without visible bubble interlinking on the grain faces. Analysis of these tests and development of a new advanced model for intergranular gas transport based on these experimental observations will be presented in this paper (Part 1).

The new model is implemented in the MFPR (Module for Fission Products Release) code developed in collaboration between IBRAE (Moscow, Russia) and IRSN (Cadarache, France) for mechanistic modelling of fission product release from irradiated UO_2 fuel [10,11], and validated against various tests (as presented in Part 2).

2. Experimental observations

In the tests [8,9] the 3 and 4 BWR cycle specimens with ≈2.4% and 2.9% burn-up, respectively, were taken from the outer pellet region (between periphery and middle), and the fractional coverage of grain faces by bubbles was evaluated from scanning electron microscopy (SEM) photographs as ≈0.06 and 0.1 [8], respectively, see Fig. 1, panels a and b.

Despite such low values of the grain face coverage, significant fractional fission gas release (up to 20–30%) during their base irradiation was measured by pin puncture tests from these specimens, Fig. 2. Therefore, a noticeable gas release from these fuel samples occurred at coverage far below the saturation value, i.e. without visible bubble interlinking on the grain faces. The irradiation temperature at the location of the specimens was not directly measured, but might be evaluated as ~1100–1250 °C from the maximum linear heat generation rates between 30 and 37 kW/m.

On the other hand, a significant burst release observed in these tests during post-irradiation annealing at 1600–1800 °C was invariably associated in Refs. [8,9] with the coverage of about 0.4–0.6 (see Table 1 from Ref. [9]) attained under various burn-

* Corresponding author. Tel.: +7 495 955 2218; fax: +7 495 958 0040.
E-mail address: vms@ibrae.ac.ru (M. S. Veshchunov).

0022-3115/$ - see front matter © 2009 Elsevier B.V. All rights reserved.
doi:10.1016/j.jnucmat.2009.03.055

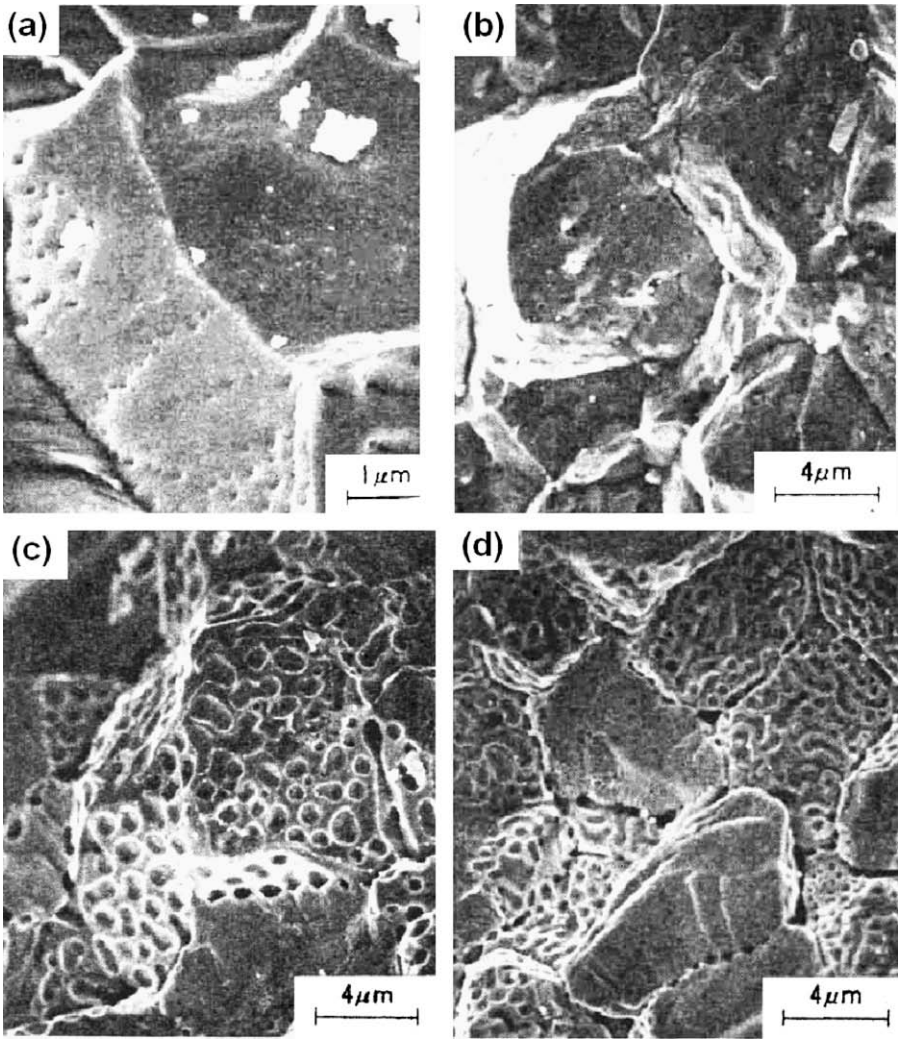

Fig. 1. Scanning electron micrographs of fuel fracture surface from Ref. [8]: (a) 2 cycle as-irradiated specimen, (b) 4 cycle as-irradiated specimen, (c) 4 cycle specimen heated up to 1800 °C, and (d) 2 cycle specimen annealed 5 h at 1800 °C.

ups and heating conditions, Fig. 1, panels c and d. A similar result was observed in the annealing tests [12], where the coverage was stabilized after a short transition period in a narrow interval 0.49–0.55 near the critical value of 0.5 (see, e.g. recent evaluation of those experimental data in Ref. [13]). Hence, interlinking of grain face bubbles at the threshold coverage value of ≈0.5 (e.g. considered in Ref. [7]) might be responsible for the secondary burst release observed in the annealing stage of the tests [8,9,12].

Therefore, from these tests it can be generally concluded that at irradiation temperatures $\leqslant 1250$ °C the formation of the interlinked bubbles network on grain faces can be significantly delayed, but this does not prevent an earlier commencement of gas release.

This conclusion can be generally confirmed by observations of fuel microstructure under transient irradiation conditions [14]. In these tests, the UO_2 fuel pins of different structure and density were base-irradiated to burn-ups from 1.5 to 4.7 at.% in PWR reactors with different levels of peak power. The transient tests were carried out in the research DR3 reactor in a water cooled rig with a coolant pressure of 70 atm to simulate PWR and BWR conditions.

Post-irradiation examinations of the fuel pellets in these tests showed that formation of edge tunnels and commencement of significant gas release measured (from the radial distribution of retained Xe by X-ray fluorescence (XRF) and electron microprobe analysis (EPMA) methods) at different radial positions of fuel pellets took place at relatively low ($\leqslant$0.1–0.2) coverage of grain boundaries by face bubbles that were not interlinked (as can be seen from Figs. 7–12 and Table 2 of Ref. [14]), in a qualitative agreement with the observations under steady irradiation conditions [8,9].

However, in analysis of these tests one must take into consideration that under transient conditions the magnitude of the local mechanical restraint pressure in the fuel and the existence of macroscopic pressure gradients are important in determining the behaviour of the gas bubbles on the grain faces. It was shown in Ref. [14] that the magnitude of the mechanical restraint stresses appeared to have been particularly high during the transient test (up to 100 MPa). For this reason, direct application of the current model to the transient tests is not attempted in this paper, owing to uncertainties in evaluation of the mechanical restraint forces.

3. Analysis of experimental data

To explain this effect observed under steady state [8,9] irradiation conditions one should consider an input in the total gas release of the diffusion transport of gas atoms on grain faces in presence of grain boundary traps (bubbles). This diffusion transport apparently becomes dominant in the lack of a network of interconnected grain face bubbles. Usually the diffusion process

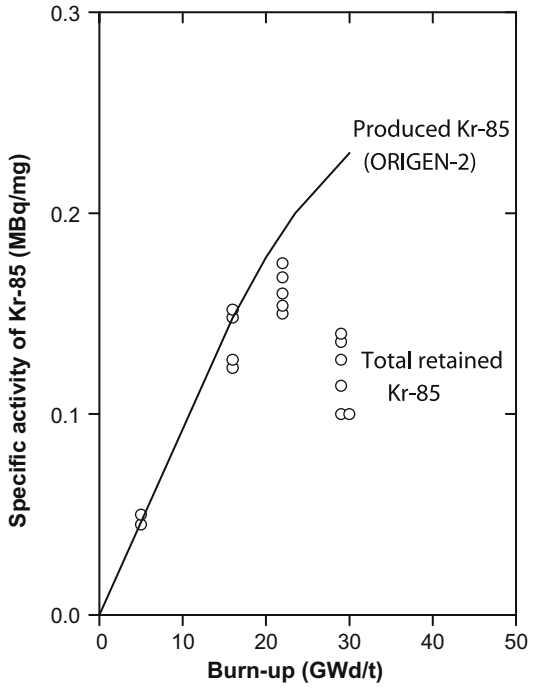

Fig. 2. ^{85}Kr concentrations in UO_2 as a function of burn-up measured in Ref. [8].

is considered only in evaluation of the grain face bubble size [15–17] and/or estimation of the incubation period for saturation coverage [1,2], since it is assumed that practically all the gas diffused from grains to grain boundaries is collected by the growing grain face bubbles and only a negligible part is transported to grain edges (before interlinking of grain bubbles). This assumption was apparently supported by the theoretical analysis [18] that showed that the sink strength of the grain face periphery (edges) became (after some initial time interval) negligibly small in comparison with the total sink strength of the growing grain face bubbles. A similar conclusion was later derived in Ref. [19].

However, these results can be strongly violated if one additionally takes into account resolution of gas atoms from face bubbles back to the grain matrix (not considered in Ref. [18]), that may essentially redistribute the diffusion flux from grains among different sinks on grain faces.

Indeed, as shown in Ref. [20] re-dissolved atoms are knocked some distance δ from the grain boundary into the grain, whence they may proceed to diffuse again. The built-up concentration barrier c_δ of the resolution layer turns out as a natural boundary condition at the resolution layer boundary δ for the intragranular diffusion problem, as recommended in Ref. [15] instead of zero boundary condition in the simplified model with no resolution effect taken into account. It reduces the diffusion flux from the grain Φ_{dif}, on the one hand, and determines the net flux of atoms deposited on the grain boundary $\Phi_\delta \approx D_g c_\delta/\delta$, on the other hand [20]. This flux Φ_δ should counterbalance the resolution flux back into the grain Φ_{res} and, in accordance with the flux matches $\Phi_\delta = \Phi_{dif} + \Phi_{res}$ (see below Section 4.2), may essentially exceed the "source term" Φ_{dif} from the grain. Namely this flux Φ_δ should be redistributed among various grain face sinks (face bubbles and edges) rather than the source term flux Φ_{dif}.

Neglecting such an effect in Ref. [18] resulted in underestimation of the grain boundary diffusion flux to edges. On the other hand, gas atom resolution from the grain faces was studied in some other papers (e.g. [1,15,20]), however the grain face diffusion transport to edges was not included in that consideration. The simultaneous consideration of various processes on the grain faces (atom diffusion, trapping by and resolution from the grain boundary bubbles) was proposed in Ref. [5] in order to reconcile various approaches. However, some simplifications of the model adopted for numerical analysis of coupled equations for intra- and intergranular transport apparently prevented the author [5] from important conclusions concerning essential role of atomic grain face transport to edges in the course of face bubbles growth. For this reason, in the subsequent paper [19] the author concluded that the contribution of grain boundary diffusion to fission gas release on the pellet scale is strongly inhibited as soon as the aerial coverage of the grain boundary traps is about 1%, and consequently a simplified or alternative model for the inter-granular behaviour of fission products (FP) was further developed.

In the papers of the present authors [21,22] an essential role of the grain face diffusion transport in the gas release mechanism was highlighted, in order to explain the above mentioned [8,9] and some other observations. For this purpose a completely self-consistent scheme for analysis of diffusion and resolution processes in the grain and grain faces was considered. In particular, it was shown that "circulation" of gas atoms collected by growing intergranular bubbles from the grain face and then returned back (by the resolution process) into the grain matrix, made bubbles much less effective sinks for gas atoms in the course of their growth saturation (i.e. approaching a balance among absorbed and re-emitted atoms) and thus continuously increased a fraction of the source term flux from grain bulk eventually transported to edges. Specifically, this leads to a natural conclusion that in the case of the complete balance between absorbed and re-emitted atoms leading to cessation of the face bubble growth (before their interlinking), ≈100% of the source term flux will be transported to grain edges via grain face diffusion process. This model is presented in detail and further improved in the next Section 4.

4. Model description

4.1. Intergranular bubbles

Three intergranular bubble types are considered following [1]:

- the grain face bubbles covering the grain faces with the surface concentration ρ_f,
- the edge bubbles located at grain edges, and
- the corner bubbles located at the grain corners (one bubble per corner).

The grain face lenticular bubbles are formed by intersection of two spherical surfaces of radius R_f and hence have a circular projection with the projected circular radius $R_f \sin\theta$, where $\theta \approx 50°$.

The edge bubbles are considered as cigar-shaped formed by intersection of three spherical surfaces. The corner bubbles with the shape constructed by intersection of four spherical surfaces can be considered with a reasonable accuracy as spherical ones. However, for simplicity the edge and corner bubbles will be further considered as indistinguishable and the peripheral porosity will be represented only by one kind (edge) of the bubbles (see details in Part 2).

The volume V_i of the type i bubble is calculated as [23]:

$$V_i = \frac{4}{3}\pi R_i^3 f_i(\theta), \tag{1}$$

where R_i is the bubble curvature radius, subscript i specifying bubble type; the correction factors f_i will be presented in Part 2.

The curvature radii for all bubble types are calculated assuming their equilibration:

$$\left(\frac{2\gamma}{R_i}+p_h\right)V_i f_i(\theta)=N_i k_B T, \tag{2}$$

where γ is the surface tension, k_B is the Boltzmann constant, T is the temperature, N_i is amount of gas atoms in the bubbles, the Van der Waals corrections for relatively large bubbles ($R_i > 5$ nm) being neglected.

4.2. Mean field approximation

In the mean field approximation it is assumed that the face bubbles have equal sizes and are randomly distributed over the grain boundary. Correspondingly, the averaged resolution flux from the face bubbles $\Phi_{res}^{(f)}$ is considered as uniform, but generally different (owing to different bubble sizes) from that at the peripheral zone of the grain boundary, $\Phi_{res}^{(e)}$, where edge and corner bubbles are located.

As above explained (see Section 3), re-dissolved atoms are knocked some distance δ from the grain boundary into the grain and create the built-up concentration barrier c_δ [20], which sets a natural boundary condition at the resolution layer boundary δ for the intragranular diffusion problem, as proposed in Ref. [15]. Owing to the difference between the resolution fluxes from the edge and face bubbles, $\Phi_{res}^{(e)} \neq \Phi_{res}^{(f)}$, the built-up concentration barriers of the resolution layer will be also different in these zones, $c_\delta^{(f)} \neq c_\delta^{(e)}$. As a result, the flux depositing on the grain boundary, which can be estimated from relation:

$$\Phi_\delta^{(f,e)} \approx D_g c_\delta^{(f,e)}/\delta, \tag{3}$$

is not completely uniform and has different values in the central and peripheral zones of the grain faces: $\Phi_\delta^{(e)} \neq \Phi_\delta^{(f)}$.

If one considers the central and peripheral zones of the grain face independently, neglecting their mutual influence on each other, then, owing to flux matches in these zones, $\Phi_\delta^{(f,e)}$ will be a sum of the diffusion flux from the grain, $\Phi_{dif}^{(f,e)}$, and the irradiation induced resolution flux from the face (edge) bubbles, $\Phi_{res}^{(f,e)}$:

$$\Phi_\delta^{(f,e)} = \Phi_{dif}^{(f,e)} + \Phi_{res}^{(f,e)}.$$

However, it can be shown (in the result of the model calculations presented in Part 2) that in this case the edge bubbles grow up more intensively than the face bubbles. For this reason, resolution flux (per unit square) from the edge bubbles is also higher than that from the face bubbles, thus, the built-up concentration barrier $c_\delta^{(e)}$ in the peripheral zone will be higher than $c_\delta^{(f)}$ in the central zone. This will lead to an additional diffusion flux in the resolution boundary layer from the peripheral to the central zone and, thus, to partial redistribution of $\Phi_{res}^{(e)}$ between the peripheral and central zones. Therefore, considering the peripheral zone, in the simplest approach one should take into account that only some part γ_e of the resolution flux $\Phi_\delta^{(e)}$ contributes to the flux matching condition:

$$\Phi_\delta^{(e)} = \Phi_{dif}^{(e)} + \gamma_e \Phi_{res}^{(e)}, \tag{4}$$

where $\gamma_e < 1$ is the new model parameter.

The corresponding input from the edge bubbles, $\Phi_{res}^{(e)}(1-\gamma_e)\varphi_e/(1-\varphi_e)$, should be included into the flux matches for the face bubbles, which accordingly takes the form:

$$\Phi_\delta^{(f)} = \Phi_{dif}^{(f)} + \Phi_{res}^{(f)} + \Phi_{res}^{(e)}(1-\gamma_e)\varphi_e/(1-\varphi_e), \tag{5}$$

where φ_e is the coverage of the grain boundary with the edge bubbles (see the next Section 4.3). Note that in the opposite case, $c_\delta^{(f)} > c_\delta^{(e)}$, one should introduce, instead of γ_e, a similar parameter γ_f characterising partial redistribution of $\Phi_{res}^{(f)}$ to the peripheral zone.

The diffusion flux from the grain determined by different boundary conditions, $c_\delta^{(f)} \neq c_\delta^{(e)}$, also cannot be completely uniform. However, the difference between $c_\delta^{(f)}$ and $c_\delta^{(e)}$ is generally small in comparison with the gas atom concentration c_0 in the central part of the grain, $c_\delta^{(e)} - c_\delta^{(f)} \ll c_0$, therefore, in a good approximation the difference between the two diffusion fluxes can be neglected:

$$\Phi_{dif}^{(e)} \approx \Phi_{dif}^{(f)} = \Phi_{dif}. \tag{6}$$

For that reason, Φ_{dif} determined as the flux of atoms per unit square of the grain boundary, can be searched as a spherically symmetric solution of the diffusion equation for gas atoms in the grain (as it is realized in the MFPR code [10,11]).

The resolution fluxes from the edge and face bubbles are calculated as:

$$\Phi_{res}^{(e)} = \omega_e Y_e/\varphi_e, \tag{7}$$

$$\Phi_{res}^{(f)} = \omega_f Y_f/(1-\varphi_e), \tag{8}$$

where $Y_{f,e}$ is the total number of gas atoms in the face (edge) bubbles per unit square of a grain boundary and $\omega_{f,e}$ is the kinetic parameter of irradiation induced resolution from the face (edge) bubbles (see Part 2).

4.3. Fluxes deposited on the grain boundary

The averaged over the grain surface fluxes of gas atoms, which are directly captured by the face and edge bubbles, in the mean field approximation are calculated as $\Phi_\delta^{(f)}\varphi_f$ and $\Phi_\delta^{(e)}\varphi_e$, respectively, where $\varphi_{f,e} = S_{f,e}\rho_{f,e}$ is the coverage of the grain boundary with the face (edge) bubbles; $S_{f,e}$ and $\rho_{f,e}$ are the area of the face (edge) bubble projection on the grain surface and the face (edge) bubble surface density, respectively. The remaining part of the net flux deposited on the grain boundary unoccupied with the bubbles, $\Phi_\delta^{(f)}(1-\varphi_f-\varphi_e)$, is redistributed by surface diffusion among different sinks (described in the next Section 4.4).

Evaluation of the projection areas and surface densities for the face and edge bubbles will be presented in Part 2.

4.4. Sink strengths and diffusion transport

Owing to an extremely high ratio of the gas atom diffusion coefficients on grain faces D_f and in the grain matrix D_{gr}, which is usually believed to be of the same order of magnitude as that for the uranium self-diffusion coefficients, $D_f/D_{gr} \simeq 10^5$ [24], one can apply results of the steady-state consideration of the grain face diffusion problem [18] to calculate the face bubbles and edges sink strengths in the mean field approximation:

$$(k_f R_s)^2 = \frac{8\left(1-\varphi_f\right)}{-(1-\varphi_f)(3-\varphi_f)-2\ln\varphi_f}, \tag{9}$$

$$(k_e R_{face})^2 = 2k_f R_{face}\frac{I_1(k_f R_{face})}{I_2(k_f R_{face})}, \tag{10}$$

where d_{gr} is the grain diameter, $R_{face} = d_{gr}/\sqrt{14}$ is the effective radius of the grain face, $R_s = (\pi\rho_f)^{-1/2}$ is the radius of a concentric sink-free region which surrounds each face bubble in the plane of the grain boundary, I_1 and I_2 represent the first and the second modified Bessel functions of the first kind, respectively.

The values k_f^2 and k_g^2 determine the relative sinks of the surface diffusion flux: a part $k_f^2/(k_f^2+k_e^2)$ of the flux sinks to the face bubbles (and then is partially ejected back into the grain), while the residual part $k_e^2/(k_f^2+k_e^2)$ sinks to the edges.

One can see from Eq. (9) that $k_f R_s \sim 1$, if φ_f is not too small. Taking into account that $R_{face} \gg R_s$ one obtains that $k_f R_{face} \gg 1$. Therefore, owing to $I_1(x)\}/I_2(x) \to 1$ for large x values, one deduces that $k_e/k_f \approx \sqrt{2/k_f R_{face}} \ll 1$. It is just this strong inequality that prevented the authors of the papers [18,19] from conclusion

concerning the important role of the atomic grain face transport to edges in the course of grain face bubble growth (before interlinkage).

4.5. Balance equations

Balance equations for the mean surface densities (numbers of atoms per unit area of the grain surface), $Y_{f,e} = N_{f,e}\,\rho_{f,e}$, of the face and edge bubbles take the form:

$$\frac{d}{dt}Y_f = \varphi_f \Phi_\delta^{(f)} + \left(1-\varphi_e-\varphi_f\right)\Phi_\delta^{(f)}\frac{k_f^2}{k_f^2+k_e^2} - \omega_f Y_f, \tag{11}$$

$$\frac{d}{dt}Y_e = \varphi_e \Phi_\delta^{(e)} + (1-\varphi_e-\varphi_f)\Phi_\delta^{(f)}\frac{k_e^2}{k_f^2+k_e^2} - \omega_e Y_e. \tag{12}$$

The first terms in the r.h.s. of the equations describe the part of the total gas flux that is directly captured by the bubbles. The second terms describe the diffusion transport along the grain faces, redistributed in accordance with the sink strengths, Eqs. (9) and (10), among the face (Eq. (11)) and edge bubbles (Eq. (12)). The third terms describe the loss of the gas atoms due to irradiation induced resolution from bubbles.

The system of Eqs. (11) and (12) describes evolution of intergranular porosity up to the moment when corresponding saturation conditions are attained; after transformation it takes the form:

$$\frac{d}{dt}Y_{f,e} = F_{f,e}, \tag{13}$$

where

$$F_f = -\Omega_f Y_f + \Omega_e Y_e + a_f \Phi_{dif}, \tag{14}$$

$$F_e = \Omega_f Y_f - \Omega_e Y_e + a_e \Phi_{dif}. \tag{15}$$

are the total fluxes to the face and edge bubbles, respectively.

Here

$$\Omega_f \equiv \frac{1-\varphi_f-\varphi_e}{1-\varphi_e}\frac{k_e^2}{k_f^2+k_e^2}\omega_f, \quad \Omega_e = \frac{1-\gamma_e}{1-\varphi_e}a_f\omega_e,$$
$$a_e \equiv \frac{\varphi_e k_f^2+(1-\varphi_f)k_e^2}{k_f^2+k_e^2}, \quad a_f \equiv \frac{(1-\varphi_e)k_f^2+\varphi_f k_e^2}{k_f^2+k_e^2}, \tag{16}$$

where the dimensionless coefficients a_f and a_e obey the relationship: $a_f + a_e = 1$. Note that the source terms in the r.h.s. of Eqs. (14) and (15) are generally much smaller than the main competitive terms $\Omega_f Y_f$ and $\Omega_e Y_e$, if $(1-\gamma_e)$ is not too small, e.g. $\geqslant 0.1$. The tuning procedure for this parameter against the test data presented in Part 2 (Section 3), indeed yields $(1-\gamma_e) \approx 0.23$.

Formation of the network of the interconnected grain face bubbles is supposed to occur when the projected area coverage of the grain face by bubbles φ_f attains the critical (percolation) value $\varphi_f^{(cr)}$ (see Section 1), chosen in the MFPR code equal to 0.5, following [7] and in accordance with observations in the annealing tests [8,9,12] (see Section 2). The grain edge porosity interlinkage and formation of escape tunnels take place when the edge bubbles are just touching each other (the 1-d percolation threshold) at the critical value $\varphi_e^{(cr)}$, evaluated in Part 2.

In consideration of the percolation criteria, the system of balance equations takes a more general form:

$$\frac{d}{dt}Y_f = F_f\theta(\varphi_f^{(cr)}-\varphi_f), \tag{17}$$

$$\frac{d}{dt}Y_e = (F_e + F_f\theta(\varphi_f-\varphi_f^{(cr)}))\theta(\varphi_e^{(cr)}-\varphi_e), \tag{18}$$

$$\frac{d}{dt}Y_r = (F_e + F_f\theta(\varphi_f-\varphi_f^{(cr)}))\theta(\varphi_e-\varphi_e^{(cr)}), \tag{19}$$

where $\theta(x)$ is the Heaviside step function, Y_r is the amount of the released gas.

In accordance with the percolation mechanism [1], after attainment of the $1-$d percolation threshold, $Y_e = Y_e^{(cr)}$, gas release (venting) from the escape tunnels formed by interconnected edge bubbles commences. Owing to gas venting, the tunnels collapse and disintegrate in a smaller amount of bubbles. However, since these bubbles continue to grow owing to the diffusion flux from the grain boundaries, the percolation threshold and bubbles interlinkage quickly reinstate, and the processes of gas venting and tunnels collapse repeat, and so on, keeping the mean edge coverage close to the percolation threshold, while the mean bubble curvature radius R_e (along with the tunnel radius $\sim R_e$) continuously increases. Under equilibrium condition, Eq. (2), for the edge bubbles, $N_e = P_e V_e/k_B T \propto \gamma R_e^2/T$, and the threshold condition for their surface density, $\rho_e \propto R_e^{-1}$ (i.e. when they touch each other), one obtains $Y_e^{(cr)} = N_e\rho_e \propto R_e\gamma/T$, therefore, $Y_e^{(cr)}$ also continuously increases.

In a later stage, stable (with respect to surface-diffusion-driven collapse) tunnels are formed under condition that the tunnel network constitutes more than ≈6% volume swelling [1]. As explained in Ref. [25], this can occur only if the gas pressure in the tunnels equilibrates their surface curvature ($\Delta P \approx \gamma/R_e$), otherwise, they will shrink (similarly to sintering pores) until instability again breaks them up (e.g. below the critical swelling of ≈6%). This implies that $Y_e^{(cr)}$ continues to increase along with the tunnel radius growth in the late swelling stage.

From Eqs. (17), (18), and (2) it follows that in steady irradiation regime after accomplishment of the percolation condition for the grain edge bubbles, $Y_e = Y_e^{(cr)}(t)$, the steady-state values of Y_f and φ_f will be quickly attained:

$$Y_f^{(ss)} = \frac{\Omega_e Y_e^{(cr)} + a_f\Phi_{dif}}{\Omega_f} \approx \frac{\Omega_e}{\Omega_f}Y_e^{(cr)},$$
$$\varphi_f^{(ss)} = \pi R_f^2\rho_f \approx \frac{3\sin^2\theta_f}{8\gamma f(\theta_f)}k_B T Y_f^{(ss)} \propto \frac{TY_f^{(ss)}}{\gamma}. \tag{20}$$

From Eq. (20) it follows that the steady-state coverage factor $\varphi_f^{(ss)}$ can smoothly vary with time. Indeed, from Eq. (16) and equations derived in Section 4.4 it is seen that $\Omega_e/\Omega_f \sim k_f^2/k_e^2 \sim k_e \sim R_s^{-1}$, so, taking into account the above derived relationship, $Y_e^{(cr)} \propto R_e\gamma/T$, one obtains $\varphi_f^{(ss)} \sim T\Omega_e Y_e^{(cr)}/\gamma\Omega_f \propto R_e/R_s$, and therefore, $\varphi_f^{(ss)}$ can vary as a result of competition between the edge and face bubbles coalescence rates.

The steady-state values, Eq. (20), are generally below the critical ($2-$d percolation) limit. This implies that the face coverage is stabilised and gas atoms are completely transported to the grain edges by surface diffusion in the lack of the face bubbles interlink-

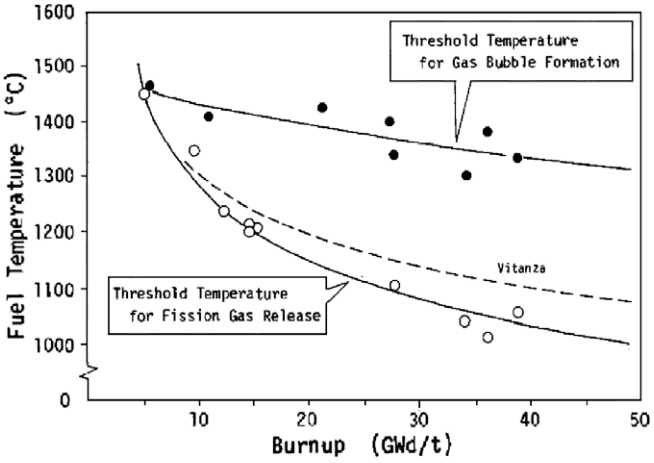

Fig. 3. Threshold temperatures for fission gas release and for bubble formation as functions of burn-up (from Ref. [28]).

age. This conclusion is in a qualitative agreement with experimental observations [8,9] (see also Fig. 3 below) and will be confirmed by numerical simulations of gas release in a wide temperature range in Part 2 (Section 3).

Note, that the above consideration is valid only for irradiation regimes for which the resolution mechanism plays a key role. On the contrary, under post-irradiation annealing conditions no steady-state coverage can be attained below the percolation threshold and thus the gas release can be generally associated with the percolation network (as discussed in Section 2).

4.6. Preliminary validation

Preliminary validation of the model after its implementation in the MFPR code against the tests [8,9] confirmed that a noticeable gas release from these fuel samples might occur at low coverage far below the critical value of 0.5 and without visible bubble interlinking on the grain faces, see Refs. [21,22]. More detailed validation of the improved model will be presented in Part 2.

5. Discussion of tests with MOX fuel

In the mixed-oxide fuel (MOX) fuel irradiated under nominal conditions in French PWR rods (where the centre-line temperatures as calculated lied in the range from 1000 to 1200 °C) with examinations by optical microscope, microprobe analyser, and scanning electron microscope, it was not possible to observe intergranular bubbles, even in rods with high gas release (up to 4-5%) [26].

In order to explain high release values and decrease of the gas content in the U-rich matrix measured in the central part of the pellet, assumption is made in Ref. [26] that in the MOX fuel, there is a strong enhancement of the kinetics of xenon migration in the grain boundaries. This assumption is based on the experiments on interdiffusion of PuO_2 in UO_2 [27] which show that the cation diffusion coefficients in grain boundary is much higher (about 2 orders of magnitude) in the presence of Pu. As xenon diffusion is related to cation diffusion, it was assumed a similar evolution of the Xe diffusion coefficients.

A similar behaviour was observed in the tests [28] with the MOX fuel from Japanese fast reactor JOY0 MK-I, where precipitation of intergranular gas bubbles in the central zone (so-called "gas bubble region") of the fuel pellets under reactor irradiation conditions occurred significantly later than commencement of gas release from this zone (detected by puncturing tests). At 30 GWd/t, for example, fission gas release takes place at a local fuel temperature of 1080 °C, and face bubble formation becomes visible with the optical microscope above 1360 °C. More generally, the threshold temperatures for fission gas release and for bubble formation as functions of burn-up are presented in Fig. 3 (in comparison with the fission gas release threshold curve from Ref. [29] – dashed line). Furthermore, scanning electron micrographs of the "gas bubble region", showing bubbles at grain faces and tunneling along the grain edges, give direct evidence that gas release through the open edge tunnels occurred at relatively low coverage of grain faces (below the percolation threshold), Fig. 4.

Therefore, for modelling of the MOX fuel irradiated in PWR and fast reactors, the new model for gas transport on grain boundaries becomes especially important. This model allows explanation of gas release without network of interconnected face bubbles (as observed in the above described tests), and thus, after certain modifications can be applied also to the MOX fuel.

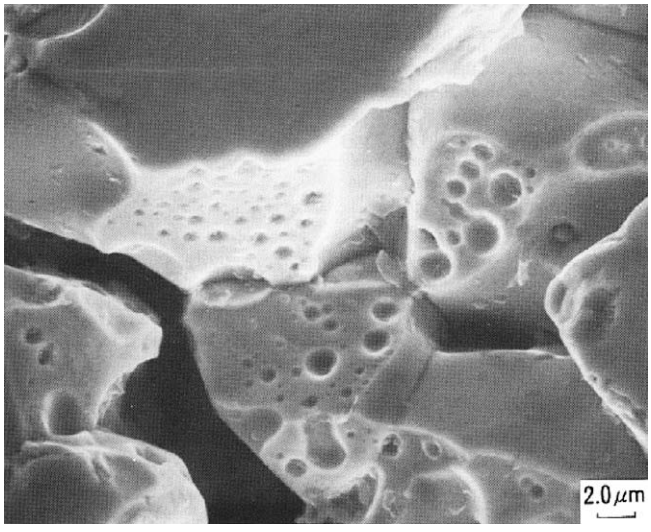

Fig. 4. Scanning electron micrograph of JOY0 MK-I fuel showing gas bubbles at the grain surface and tunneling along the grain edge in the gas bubble region with significant gas release (from Ref. [28]).

6. Conclusions

The advanced model for the grain face transport of gas atoms self-consistently takes into consideration the effects of atom diffusion on the grain surface, their trapping by and irradiation induced resolution from intergranular bubbles. It is shown that "circulation" of gas atoms collected by growing intergranular bubbles from the grain face and then returned back (by the resolution process) into the grain matrix, makes intergranular bubbles much less effective sinks for gas atoms, since it decreases their growth (i.e. approaching a balance among absorbed and re-emitted atoms) and thus continuously increases a fraction of the source term flux (i.e. diffusion flux from grains to grain faces) eventually transported to the grain edges.

In particular, this allows prediction that a noticeable gas release from the fuel commences when the grain face coverage is far below the critical value manifested by formation of a network of interconnected grain face bubbles, in accordance with the experimental observations of the UO_2 fuel behaviour under steady irradiation conditions.

An important application of the new model for description of significant gas release from the MOX fuel without visible formation of the face bubbles, observed in PWR and fast breeder reactors at temperatures below ≈1450 °C, is outlined.

Numerical simulations of gas release associated with the intergranular porosity evolution under irradiation conditions in a wide temperature range by the new model implemented in the MFPR code will be presented in Part 2.

Acknowledgements

This work was supported by IRSN, Cadarache (France) under the Contract on the mechanistic code MFPR development; the personal support and collaboration of Dr R. Dubourg and Dr P. Giordano (IRSN) are highly appreciated. The authors thank Dr V. Ozrin (IBRAE) for valuable discussions and assistance.

This work was also supported by the Russian Foundation for Basic Research (RFBR), which is greatly acknowledged by the authors.

References

[1] R.J. White, M.O. Tucker, J. Nucl. Mater. 118 (1983) 1.
[2] K. Forsberg, A.R. Massih, J. Nucl. Mater. 135 (1985) 140.
[3] C.C. Dollins, F.A. Nichols, J. Nucl. Mater. 91 (1976) 143.

[4] T. Kogai, J. Nucl. Mater. 244 (1997) 131.
[5] P. van Uffelen, Development of a new fission gas release and fuel swelling model, in: Enlarged Halden Programme Group Meeting, Lillehammer (Norway), 1998, HPR-349.
[6] C. Ronchi, J. Nucl. Mater. 15 (1976) 311.
[7] T.J. Heames, D.A. Williams, N.E. Bixler, A.J. Grimley, C.J. Wheatley, N.A. Johns, P. Domogala, L.W. Dickson, C.A. Alexander, I. Osborn-Lee, S. Zawadzki, J. Rest, A. Mason, R.Y. Lee, VICTORIA: A Mechanistic Model of Radionuclide Behaviour in the Reactor Coolant System Under Severe Accident Conditions, NUREG/CR-5545, 1992.
[8] K. Une, S. Kashibe, J. Nucl. Sci. Technol. 27 (1990) 1002.
[9] S. Kashibe, K. Une, J. Nucl. Sci. Technol. 28 (1991) 1090.
[10] M.S. Veshchunov, V.D. Ozrin, V.E. Shestak, V.I. Tarasov, R. Dubourg, G. Nicaise, Nucl. Eng. Des. 236 (2006) 179.
[11] M.S. Veshchunov, R. Dubourg, V.D. Ozrin, V.E. Shestak, V.I. Tarasov, J. Nucl. Mater. 362 (2007) 327.
[12] I. Zacharie, S. Lansiart, P. Combette, M. Trotabas, M. Coster, M. Groos, J. Nucl. Mater. 255 (1998) 85.
[13] M.S. Veshchunov, J. Nucl. Mater. 374 (2008) 44.
[14] C.T. Walker, P. Knappik, M. Mogensen, J. Nucl. Mater. 160 (1988) 10.
[15] J.A. Turnbull, J. Nucl. Mater. 50 (1974) 62.
[16] J.A. Turnbull, M.O. Tucker, Philos. Mag. 30 (1974) 47.
[17] M.H. Wood, J. Nucl. Mater. 119 (1983) 67.
[18] J.R. Matthews, M.H. Wood, J. Nucl. Mater. 91 (1980) 241.
[19] P. van Uffelen, Assessing the contribution of grain boundary diffusion to fission gas release in nuclear fuel. in: Enlarged Halden Programme Group Meeting, Loen (Norway), 1999.
[20] M.V. Speight, Nucl. Sci. Eng. 37 (1969) 180.
[21] M.S. Veshchunov, A.V. Berdyshev, V.I. Tarasov, Development of Fission Gas Bubble Models for UO_2 Fuel in Framework of MFPR Code, Preprint IBRAE-2000–08, Moscow, 2000.
[22] A.V. Berdyshev, M.S. Veshchunov, Modelling of Grain Face Diffusion Transport and Swelling in UO_2 Fuel, Preprint IBRAE-2002–14, Moscow, 2002.
[23] P.J. Clemm, J.C. Fisher, Acta Metall. 3 (1955) 70.
[24] G.B. Alcock, R.J. Hawkins, A.W.D. Hills, P. McNamara, Paper SM-66/36, IAEA, Symp. Thermodynamics, Vienna, 1965, p. 57.
[25] F.A. Nichols, J. Nucl. Mater. 148 (1987) 92.
[26] Y. Guerin, J. Noirot, D. Lispaux, C. Struzik, P. Garcia, P. Blainpain, G. Chigne, Microstructure evolution and in-reactor behaviour of MOX fuel, in: Proceedings of the International Topical Meeting on LWR Fuel Performance, 10–13 April 2000, Park City, Utah, USA, p. 706.
[27] S. Mendez, Etude de l'interdiffusion U-Pu applique au combustible MOX, Thesis Universite Aix-Marseille, 1995.
[28] S. Ukai, T. Hosokawa, I. Shibahara, Y. Enokido, J. Nucl. Mater. 151 (1988) 209.
[29] C. Vitanza, E. Kolstad, U. Graziani, in: ANS Topical Meeting on Light Water Reactor Fuel Performance, Portland, Oregon, USA, 1979.